Palaeogeography, Palaeoclimatology, Palaeoecology 600 (2022) 111074

Contents lists available at ScienceDirect

Palaeogeography, Palaeoclimatology, Palaeoecology

journal homepage: www.elsevier.com/locate/palaeo

Biomarker evidence for deforestation across the Triassic-Jurassic boundary in the high palaeolatitude Junggar Basin, northwest China

Xiaoyu Zhang [a,b,1], Peizong Lv [a,b,1], Linhao Fang [a,b,*], Guangli Wang [a,b,*], Yuanzheng Lu [c], Shenghui Deng [c], Han Yang [d], Yanan Fang [e], Hongjia Li [a,b], Xinzhi Zhang [a,b], Yue Sun [a,b], Yuxuan Chen [a,b], Shengbao Shi [a,b]

[a] College of Geosciences, China University of Petroleum (Beijing), Beijing 102249, China
[b] State Key Laboratory of Petroleum Resource and Prospecting, China University of Petroleum (Beijing), Beijing 102249, China
[c] Research Institute of Petroleum Exploration and Development, PetroChina, Beijing 100083, China
[d] Key Laboratory of Earthquake Geodesy, CEA, Wuhan 430071, China
[e] State Key Laboratory of Palaeobiology and Stratigraphy, Nanjing Institute of Geology and Palaeontology, Chinese Academy of Sciences, Nanjing 210008, China

ARTICLE INFO

Editor: H. Falcon-Lang

Keywords:
End-Triassic mass extinction
Terrestrial
Wildfire
Higher plants biomarkers
Fern spikes

ABSTRACT

The end-Triassic mass extinction (ETE), one of the five largest mass extinctions, occurred at 201.6 Ma. It was characterized by dramatic declines in marine and terrestrial ecosystems and was approximately synchronous with the eruption of the Central Atlantic Magmatic Province (CAMP). Loss of marine biodiversity is linked to extreme global warming while the cause of floral destruction in terrestrial ecosystems remains open to debate. In this paper, biomarker records of higher plants are reported from terrestrial facies in the Haojiagou section of the high palaeolatitude Junggar Basin, northwest China. Strata around the ETE interval are marked by sharp increases in the abundances of cadalene, retene, pimanthrene and furans, which are synchronous with "fern spikes". These results are interpreted as indicating the demise of land vegetation and the enhanced burial of higher plants, consistent with palynological evidence for the loss of floral diversity. The fluctuations in the abundance of *n*-alkanes series and conversion of *n*-alkanes peak patterns coincide with wildfires indicated by polycyclic aromatic hydrocarbons. Based on integrated stratigraphic correlation, the increased burial of higher plants, wildfires and CAMP volcanism are synchronous both in the Haojiagou section and other classic Triassic-Jurassic boundary sections globally. We propose that widespread deforestation may be due to CAMP-derived acid rain and the rapid and large-scale demise of vegetation may have provided moisture-free fuels for wildfires.

1. Introduction

The end-Triassic mass extinction (ETE) is one of the five largest mass extinctions in the past 600 million years and witnessed the loss of 50% marine and terrestrial genera (Raup and Sepkoski, 1982; Mcghee et al., 2013; Dunhill et al., 2018; Wignall and Atkinson, 2020). The Mid-Atlantic Ocean opened and shaped the global pattern of plate tectonics for subsequent 200 million years (de Lamotte et al., 2015; Peace et al., 2019). It is implied that the extreme paleoclimates took place, such as a fourfold rise in atmospheric CO_2 concentrations (Beerling and Berner, 2002; Steinthorsdottir et al., 2011; Schaller et al., 2011, 2012) and a ~ 3 to 4 °C global warming (McElwain et al., 1999; Bonis and Kürschner, 2012; Landwehrs et al., 2020), global sea level fluctuations (Lindström and Erlström, 2006), ocean acidification and anoxia (Hautmann et al., 2008; Greene et al., 2012; Jaraula et al., 2013) and widespread wildfire activities (Belcher et al., 2010; Petersen and Lindström, 2012; Song et al., 2020; Zhang et al., 2020). The initial trigger to the series of events was attributed to volcanism of the Central Atlantic Magmatic Province (CAMP) (Lindström et al., 2021).

Fowell and Olsen (1993) first revealed high abundances of fern sporopollen from Triassic-Jurassic boundary (TJB) sediments in the Newark basin, so called "fern spike". This sharp increase in fern sporopollen has been widely reported in China (Lu and Deng, 2009), Poland (Pieńkowski et al., 2012), Germany (van de Schootbrugge et al., 2009), North America (Fowell and Olsen, 1993; Lucas and Tanner, 2007) and Greenland (McElwain et al., 2009). Biomarker datasets against

* Corresponding author at: College of Geosciences, China University of Petroleum (Beijing), Beijing 102249, China.
E-mail addresses: linhao.fang@cup.edu.cn (L. Fang), sydxwgl@cup.edu.cn (G. Wang).
[1] X.-Y.Z., P.-Z.L., and L.-H. F contributed equally to this work.

https://doi.org/10.1016/j.palaeo.2022.111074
Received 1 January 2022; Received in revised form 17 May 2022; Accepted 17 May 2022
Available online 20 May 2022

continuous stratigraphic sequences can potentially provide much higher resolution stratigraphic records than those of fossil plants or palynological documents. Biomarkers are complex molecular fossils derived from biochemicals, particularly lipids, in once-living organisms (Eglinton et al., 1964; Eglinton and Murphy, 1969). High-molecular-weight *n*-alkanes with odd-number predominance, cadalene, retene, pimanthrene and furans, which are indicative of higher plants (Simoneit, 1977; Wakeham et al., 1980; Simoneit et al., 1986; van Aarssen et al., 1990; Jiang et al., 1998; Grice et al., 2005; Peters et al., 2005; Song et al., 2020), are geochemically significant. Therefore, biomarkers can faithfully reconstruct the floral changes but few are reported to reveal the ETE vegetation turnovers at a high palaeolatitude terrestrial ecosystems.

Here, we try to decode the flora's response to the ETE and CAMP recorded at a high palaeolatitude in the Junggar Basin, northwestern China. For this reason, we selected biomarkers including *n*-alkanes, cadalene, retene, pimanthrene and furans, and provide the high-resolution evidence of their abundance changes.

2. Geological setting and stratigraphy

The Junggar Basin, occupying approximately 136,000 km^2 and adjacent areas of the Tianshan and Altai mountains (Sha et al., 2015), was situated at palaeolatitude about 60° N during the Late Triassic (Fig. 1A). The basin remained active since the late Early Permian. As suggested by Cai et al. (2000), the Junggar block was uplifted and transformed into an inner craton basin at the end of the Triassic. Subsequently, a lacustrine depositional system widely occurred during the Early to Middle Jurassic (Fang et al., 2004; Li et al., 2007).

The Haojiagou section is located about 50 km southwest of Urumqi, Xinjiang Province, northwest China (Sha et al., 2015) (Fig. 1B). The stratigraphic succession covers from the Late Triassic to Jurassic (Fig. 2). The strata studied in this paper comprises the upper Haojiagou and lower Baodaowan formations (Fig. 1C). Sediments of the upper Haojiagou Formation consist of yellow-green and gray-green sandstones, conglomerates and mudstones interbedded with coal seams and siderite concretions. The sedimentary rocks of the lower Baodaowan Formation mainly consist of gray-white, light gray-green conglomerate, light yellow-green, gray-green medium-coarse sandstone, gray-green fine

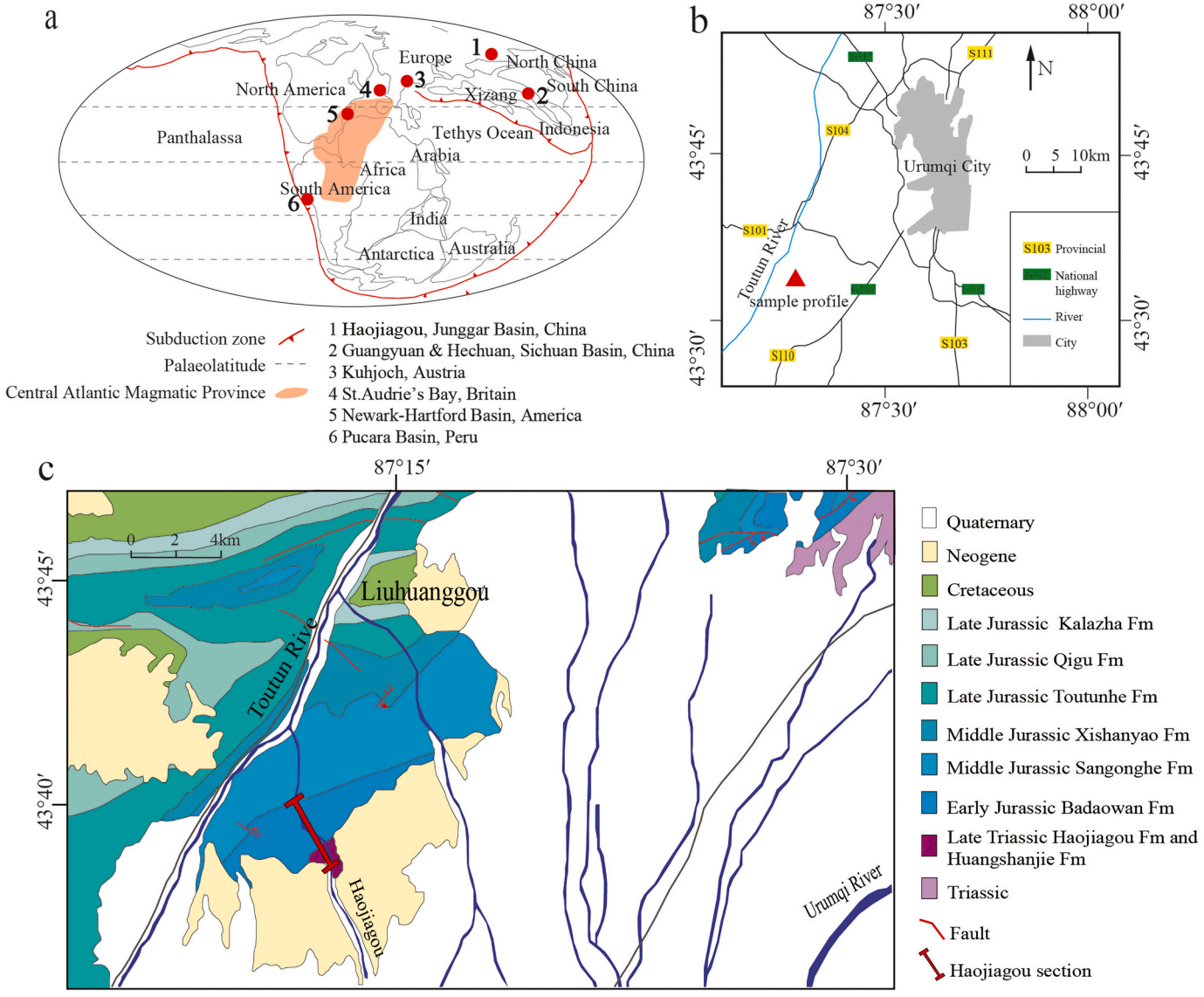

Fig. 1. Paleogeographic and geological maps of the Junggar Basin. (a) Global paleogeography during Triassic-Jurassic transition, including the distribution of the Central Atlantic Magmatic Province (CAMP) and positions of the investigated profiles. (b) Traffic map and location of the Haojiagou section. (c) Geological map around the Urumqi city area showing the position of the Haojiagou section (Modified from Sha et al., 2015).

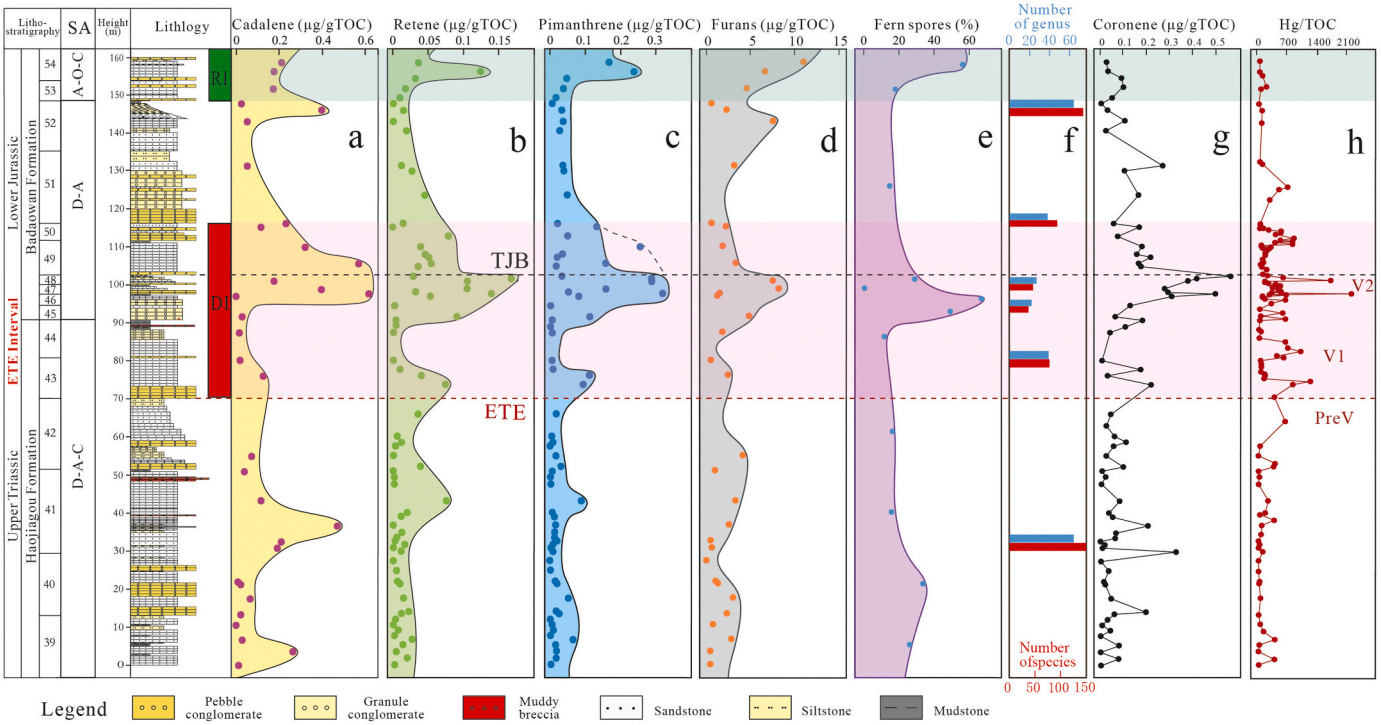

Fig. 2. Stratigraphic distribution of biomarkers, fern spores, spore genus and species, coronene and Hg/TOC content in the Haojiagou section. SA = Sporomorph assemblage zone, D-A-C = *Dictyophyllidites-Aratrisporites-Cycadopites*, D-A = *Dictyophyllidites-Alisporites*, A-O-C = *Alisporites-Osmundacidites-Cyathidites*. (a)-(d) concentration of cadalene, retene, pimanthrene and furans respectively, (e) content of fern spores (Lu and Deng, 2009), (f) number of genus and species of sporopollen (Zhang et al., 2022 under review), (g) coronene concentration and (h) Hg/TOC content (Fang et al., 2022 under review). Cadalene, retene, pimanthrene and coronene broadly respond to the deforestation interval (DI) zone. The major peaks of cadalene, retene, pimanthrene and furans in the DI zone are synchronously consistent with a distinct fern peak, loss of floral diversity, maximums of coronene and Hg/TOC. The consistence is inferred that the enhanced input of higher plants (indicated by cadalene, retene, pimanthrene and furans, and loss of floral diversity) and enhanced wildfires (indicated by coronene) are triggered by the CAMP volcanisms (indicated by Hg/TOC). The peaks of retene, pimanthrene, furans and fern spores, and the increasing floral diversity in the recovery interval (RI) zone may suggest a recovery of higher plants in the terrestrial ecosystems.

sandstone, siltstone, intercalated gray mudstone, and partial coal seams. The bed number in this study is after the scheme from Deng et al. (2010). The interval between ETE and TJB approximately lies between Bed 43 and Bed 48 (Deng et al., 2010; Fang et al., 2021).

Terrestrial TJB sections have primarily been dated by sporo-pollen, macrofossil plant remains, and vertebrate or ichnofossils (e.g. Fowell and Olsen, 1993; McElwain et al., 2007), as is the Haojiagou section. Respectively, the Haojiagou Formation was assigned to the Rhaetian stage, and the conformably overlying Baodaowan Formation to the Early Jurassic Hettangian stage (Deng et al., 2013). The Haojiagou Formation is composed of two plant fossil assemblages, including *Danaeopsis-Cladophlebis ichunensis* (containing the Late Triassic typical molecule *Danaeopsis*) and the upper *Hausmannia-Clathropteris minoria* assemblage (including *Cycadocarpidium* sp., *Cladophlebis kaoiana* and other genera and species) (Deng et al., 2013). The Badaowan Formation contains the *Clathropteris elegans-Todites princeps* assemblage at the lower part and *Coniopteris gaojiatianensis* assemblage at the upper part, as it includes the Early Jurassic common plant fossils *Todites princeps* and *Clathropteris elegans* (Deng et al., 2013).

Two sporopollen assemblages can be identified in the Haojiagou Formation and three sporopollen assemblages in lower part of the Badaowan Formation, which are followed as: (1) *Aratrusporites-Chordasporites-Nonstriate bisaccate*, (2) *Lycopodiacidites rugulatus-Nonstriate bisaccate*, (3) *Asseretospora-Dictyophyllidites*, (4) *Densoisporites-Nonstriate bisaccate*, (5) *Cyathidites-Nonstriate bisaccate* (Lu and Deng, 2009). The "fern spike" and some common Jurassic pollens are generally abundant, such as *Cyathidites* and *Densoisporites* around the boundary between the Bed 44 and Bed 45, which witnessed distinct changes in the floral types (Lu and Deng, 2009).

Based on previous biostratigraphic works, the carbon isotope stratigraphy and geochemostratigraphy improved age constraints on the study section (Fang et al., 2021). Integrated with datasets of organic carbon isotope, Hg/TOC and polycyclic aromatic hydrocarbons (PAHs), the ETE and TJB were constrained at around the Bed 45 and Bed 49, respectively (Lu and Deng, 2009; Fang et al., 2021).

3. Sampling and experimental methods

3.1. Sampling

The sedimentary rock samples were collected in the Haojiagou section of the southern margin of Junggar Basin, Xinjiang Province. According to the various lithology of coal, mudstone, sandstone and conglomerate, the sampling interval is 10 cm, 20 cm, 30–40 cm and 40–60 cm, respectively. All the samples were collected after removing weathered surface rocks.

3.2. TOC

Rock samples were powdered (< 80 mesh) with the crusher. Then 0.1 g powder samples were selected and removed carbonate minerals with HCl: Deionized water (1:7, v/v) and 60 °C heating until reaction was complete. The samples were rinsed with deionized water to neutral and dry in a constant temperature dryer, then analyzed by LECO CS230. The experimental details refer to Fang et al., 2021.

3.3. Biomarker

Approximately 100 g powder samples were extracted with 300 mL dichloromethane for 24 h by Soxhlet extractor. The extraction was dissolved with 30 mL petroleum ether and filtered out asphaltenes. Then, the solutions were transferred to silica gel/alumina chromatography columns and separated aliphatic and aromatic compounds with 30 mL petroleum ether and 20 mL dichloromethane: petroleum ether (2:1, v/v).

The *n*-alkane analyses were carried out using a Shimadzu 2010 gas chromatography (GC) equipped with an HP-5 MS fused silica column (30 m × 0.25 mm inner diameter with a 0.25 μm film coating). The injector temperature was 300 °C and initial oven temperature was programmed from 100 °C (1 min hold), to 300 °C (25 min hold) at 4/min, isothermal for.

The saturated fractions were analyzed using an Agilent 7890 Gas Chromatograph coupled to 5975i Mass Spectrometry (GC–MS) equipped with an HP-5 MS fused silica column (30 m × 0.25 mm inner diameter with a 0.25 μm film coating). Samples were injected at 50 °C and held at that temperature for 1 min. The temperature was then raised to 120 °C at 20 °C/min, and then to 310 °C at 3 °C /min, and finally kept at 310 °C for 20 min. The aromatic hydrocarbon fractions were investigated using an Agilent 7890B Gas Chromatograph coupled to 5977 Mass Spectrometry (GC–MS) equipped with an HP-5 MS fused silica column (60 m × 0.25 mm inner diameter with a 0.25 μm film coating). The initial oven temperature was 80 °C for 1 min, and then increased at 3 °C /min to 310 °C, and finally held constant for 16 min. The internal standards of $D_{50}C_{24}$ and $D_{10}P$ were used for correction of quantitative analyses for the saturated fractions and aromatic hydrocarbon fractions, respectively. The MS was operated by electron impacting (EI) with an ionization energy of 70 eV, with simultaneous full scan (m/z 5–600) and selective ion monitoring mode. For both GC and GC–MS analysis, the carrier gas was Helium. All the experiments were completed in the State Key Laboratory of Petroleum Resource and Prospecting, China University of Petroleum (Beijing).

4. Results

4.1. Index biomarkers of higher plants

The dataset of high-resolution organic geochemical biomarkers was generated from the Haojiagou section, Junggar Basin, northwest China. The compounds derived from or associated with higher plants including cadalene, retene, pimanthrene and furans have been detected and are normalized by TOC (μg/gTOC) to reflect the relative contribution (Fig. 2).

The abundances of cadalene are in a range from 0.00 to 0.47 μg/gTOC, with 0.09 μg/gTOC in average below the Bed 46, showing fluctuations in the Beds 39, 41 and 43. While the abundance sharply increases between the base of beds 46–51 (labelled as DI zone in Fig. 2), which can be up to 0.62 μg/gTOC in the Bed 46, about 6-fold increase compared to the average abundance. Sedimentary sequence upwards, abundance of cadalene gradually decreases but turns to be an increase trend in the beds 53 to 54 (labelled as RI zone in Fig. 2).

The abundances of retene are in a range from 0.00 to 0.17 μg/gTOC, with 0.01 μg/gTOC in average below the Bed 45, where small rises take place in the Beds 41 and 43. The abundance begins to increase in the Bed 45 to 0.09 μg/gTOC, until a relatively high value in the Bed 48 to 0.17 μg/gTOC, showing a 17-fold increase relative to the average value below the Bed 45. Values sharply decrease in the end of the Bed 48, which is closely above TJB. The abundance above the Bed 50 shows a similar level to that in the beds 39–44. However, it is worth noting that a slight increase and a peak occurs in the Beds 53 and 54 up to 0.12 μg/gTOC in the RI zone, which is 12-fold compared to the average values below the Bed 45 (Fig. 2).

The abundances of pimanthrene range between 0.00 and 0.11 μg/gTOC, with 0.02 μg/gTOC in average below the Bed 45, whereas the abundances are relatively high in the Bed 41 with 0.09 μg/gTOC and Bed 43 with 0.11 μg/gTOC, showing the similar characters to retene and cadalene. The abundance significantly increases in the Bed 45 to 0.11 μg/gTOC and up to the highest 0.32 μg/gTOC in the Bed 46, presenting a 16-fold increase compared to average values below the Bed 45. Sequence upwards, the abundances decrease gradually from the Bed 48. The abundance trends above the Bed 50 are similar to the beds 39 to 44. Interestingly, the peak occurs in the Bed 54 with 0.23 μg/gTOC that coincides with peaks of retene and cadalene, which is 12-fold compared to average values below the Bed 45 (Fig. 2).

Furans includes dibenzofuran, benzonaphthofuran, phenylbenzofuran, benzobisbenzofuran, dinaphthofuran and benzophenanthrofuran. The furans abundance shows slight fluctuations below the Bed 45, with 1.63 μg/gTOC in average. A significant 5-fold increase reaches the maximum value 8.21 μg/gTOC from the Bed 45 to 48. Section upwards, it decreases above the Bed 48 and the decreasing trend is similar to that of retene and pimanthrene. However, the value begins to sharply rise from the middle part of Bed 51 and reaches the highest value 11.02 μg/gTOC in the Bed 54 across the whole section (Fig. 2).

4.2. n-alkanes

Results for *n*-alkanes of the Haojiagou section are shown in Fig. 3. It comprises three dominant groups, i.e., nC_{16} and nC_{18} homologues being assigned group 1 ($nC_{16}+ nC_{18}$), nC_{23} and nC_{25} series being assigned group 2 ($nC_{23}+ nC_{25}$), and nC_{27}, nC_{29} and nC_{31} series being assigned group 3 ($nC_{27} + nC_{29}+ nC_{31}$). Below the Bed 42, sum of group 2 is over 45% and dominates among the three groups. The sum of group 1 and group 3 dramatically increases from the Bed 42, maintaining high abundance to the Bed 50, and group 3 especially exceeds 60% in the Bed 43. Sequence upwards, the group 3 has a slight downward trend until the Bed 54. With group 1 abruptly decreasing from the beds 51 to 54 (one exceptional point at the top of Bed 52), the group 2 shows an increasing trend to the Bed 54 and returns to the same value range as below Bed 43 (Fig. 3).

Two types of peak patterns for *n*-alkanes are observed, i.e., unimodal and bimodal distribution (Fig. 3). The intervals between the beds 39–42, beds 51–54 are predominated by the unimodal pattern, which exhibits the characteristic odd-number predominance, with a main peak carbon occurring at C_{23} or C_{25} (Fig. 3e). In contrast, the beds 42–51 are characterized by the bimodal pattern, where the front-peak presents even-to-odd predominance with a main peak carbon occurring at C_{16} or C_{18}. Nevertheless, there is no obvious odd-to-even predominance in the back-peak, with a main peak carbon occurring at C_{27} or C_{29} (Fig. 3e).

5. Discussion

5.1. Anomalies of higher plants biomarkers across the ETE interval

Cadalene can originate from cadinols and cadinenes that are widely discovered in higher plants (van Aarssen et al., 1990; Nguyen et al., 2003). Retene can derive from aromatization of abietane class bioditerpenoids which occur in conifer resin (Bardhan and Sengupta, 1932; Stefanova et al., 2002). Pimanthrene is proposed to originate from pimaric acid which is a major constituent of conifer resins (Wakeham et al., 1980; Simoneit et al., 1986; Peters et al., 2005). Furan structure compounds are commonly derived from the terrestrial sediments (Sephton et al., 1999), which are involved in lignin and cellulose of vascular plants (Radke et al., 2000; Nakamura et al., 2010). These four kinds of biomarkers can be well used as indicators to source of higher plants, when the potential biases are examined and excluded. Combustion can aggravate the aromatization reactions of retene and pimanthrene and directly produce these two compounds during combustion (Simoneit et al., 2000). The increasing concentration of pyrogenic PAHs demonstrates an increase of wildfire frequency across the ETE interval in

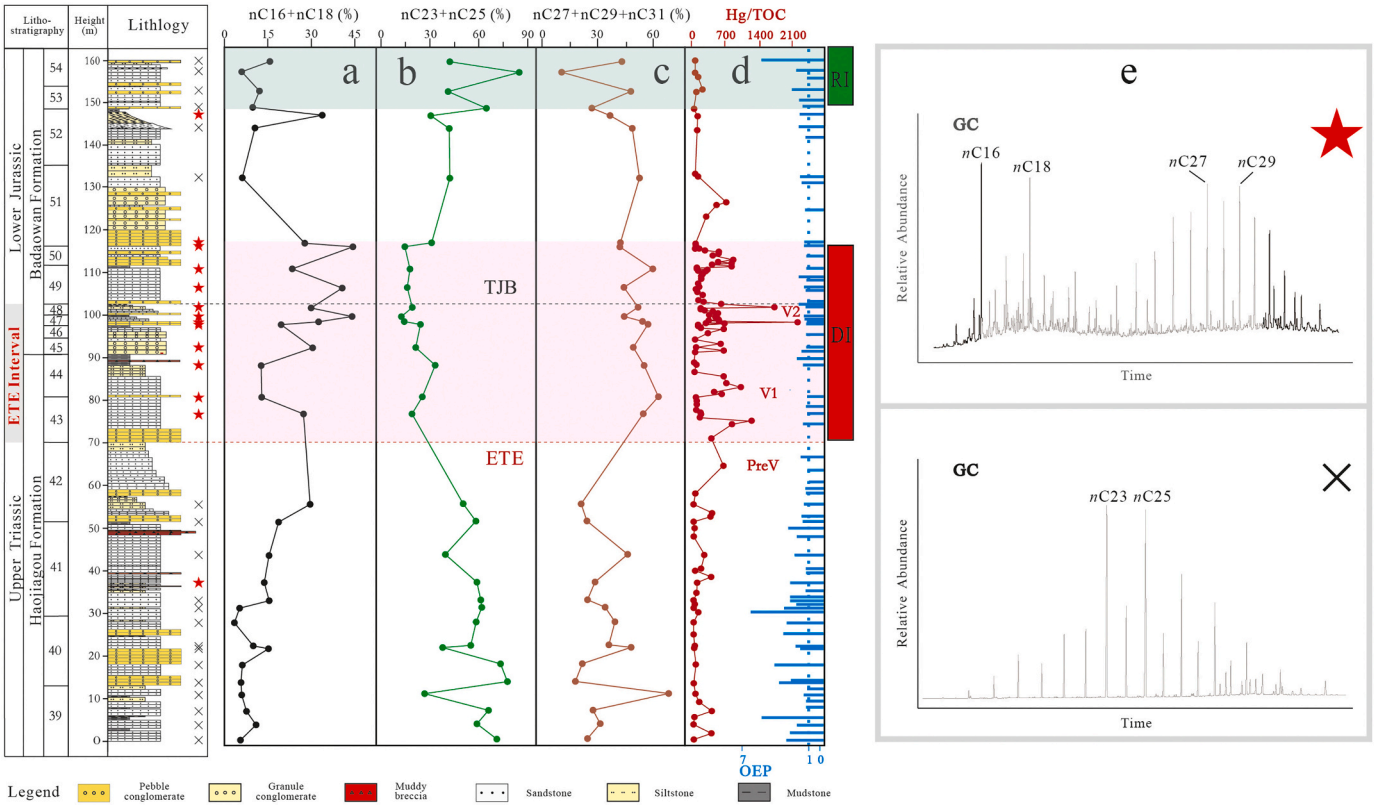

Fig. 3. Stratigraphic distribution of *n*-alkanes content, Hg/TOC, odd-to-even predominance (OEP) and two types of gas chromatograms (GC) among samples. (a)-(c) relative percentage of nC16 + nC18, nC23 + nC25 and nC27 + nC29 + nC31 respectively, (d) Hg/TOC in a red curve and OEP in blue bars, (e) two types of GC of samples which marked with red stars and black crosses along with lithological column. Abbreviations is same as Fig. 2. (For interpretation of the references to colour in this figure legend, the reader is referred to the web version of this article.)

the Haojiagou section (Zhang et al., 2020). The results of enhanced forest wildfires can aggravate the demise and burial of vegetation. Thus, the increasing abundance of retene and pimanthrene in the ETE interval (Fig. 2) could be coupled by both the enhanced deforestation and forest wildfires. The deforestation is also independently witnessed by a decreasing number of genus and species of sporopollen. The species number rapidly drops from ~150 to ~50 during the ETE interval, which suffers a decrease of two-thirds (Fig. 2f) (Zhang et al., 2022 under review).

Moreover, the geothermal history and corresponding maturity can also influence the generation of these four kinds of biomarkers. Based on well-logging temperature data, the geothermal gradients and heat flow distribution of the in the southern margin Junggar Basin were reported that the relative low geothermal gradient (<20 °C/km) and heat flow value (<35 mW/m^2), resulting in low maturity (Ro = 0.5–0.7% in most areas and <0.5% in some areas) of sedimentary organic matter from the Lower Triassic to Middle Jurassic (Ding et al., 2003; Qiu et al., 2008). Therefore, biomarker peaks in the DI and RI zones (Fig. 2) of cadalene, retene, pimanthrene and furans can exclude the factors of exceptional geothermal history and high maturity.

In addition, cadalene and retene can also be generated by microorganisms, e.g., algae, bacteria and fungi (Bordoloi et al., 1989; Jiang et al., 1994; Elias et al., 1997; Zhou et al., 2000), and retene could be biased by differential diagenesis with the sedimentary facies' changes (Grice et al., 2005). However, previous work reported that sedimentary organic matter in the Haojiagou and Baodaowan formations is dominated by kerogen type III (mainly originated from higher plants), which are also proved by palynological observations under microscope (Fang et al., 2021). The microorganisms (e.g., algae, bacteria and fungi) indicated by kerogen type II are not dominated in sedimentary organic matter. Moreover, no significant variations of sedimentary facies occur through the entire study section (~ 160 m thick) (Fig. 2), which is characterized by the shallow-water braid plain delta (Fang et al., 2016). The potential biases of exceptional microorganisms and/or differential diagenesis with changes of sedimentary facies can be ruled out in the study section.

Therefore, these biomarkers can be used as higher-plants markers to reconstruct the original signals of geological events in the Haojiagou section, when potential biased factors above are taken account or excluded. Cadalene and retene are used to indicate the abnormal input of higher plant into sedimentary organic matter and applied to reconstruct vegetation (Mizukami et al., 2013; Kaiho et al., 2016). On a long-term scale (e.g., the Upper Triassic to Middle Jurassic), the changing abundance of cadalene and retene can reflect regional climatic changes (Jiang et al., 1998). On a short-term scale (e.g., the Cretaceous-Paleogene extinction event), the rapidly increasing abundance of cadalene indicates the enhancing input of organic matter originated from higher plants, which is inferred to intensive destruction and rapid burial of terrestrial vegetation (Kaiho et al., 2016). The peak of cadalene abundance is slight displacement with those of retene and pimanthrene in the DI zone (Fig. 2), this may take account of a wider cadalene's source than that of retene and pimanthrene (Hautevelle et al., 2006; Mizukami et al., 2013). Thus, the sharp rise of cadalene abundance in beds 46 to 48 approximately corresponding to the ETE interval could be a broader relevance than abundance of retene and pimanthrene (Fig. 2), and these three biomarkers all suggest deforestation on the terrestrial ecosystems.

During the period of DI zone lasting ~270 kyr (according to astrochronology in Sha et al., 2015), the cadalene abundance is 10–15 times (beyond one-order magnitude) (Fig. 2) higher than average background values, which suggest that the vegetation was massively and rapidly buried. The peaks of retene, pimanthrene and furans in the DI zone

(Fig. 2) are consistently associated with the relatively high content of pyrogenic PAHs (e.g., coronene) during the same period (Zhang et al., 2020). All the evidence here shows that the voluminous higher plants were destructed and terrestrial ecosystem suffered drastic destruction and synchronous with enhanced wildfires in the ETE interval of the Junggar Basin. The mall rises take place in the Beds 41 and 43 of cadalene, retene and pimanthrene is likely attributed to the early stages of CAMP volcanisms in a secondary magnitude (Fig. 2).

In the zone RI (Fig. 2), the concentration of higher plants biomarker ascends once more. The floral number (from ~50 to ~150 in species, or ~ 20 to ~60 in genus) rapidly increases from beds 45 to 53 which indicates an increase of two-fold (Fig. 2f) (Zhang et al., 2022 under review). However, no records of wildfire activities are observed in the RI zone, which means the ecosystem gradually recovered and species began to multiply. These biomarker datasets demonstrate a gradual increase of higher plants contribution to sedimentary organic matter, which suggests a recovery of the ecosystem of higher plants. Similar observation is reported across the K/Pg boundary (Mizukami et al., 2013).

5.2. Wildfire activities witnessed by anomalies of n-alkanes

A simulation experiment (O'Malley et al., 1997) has shown that high-temperature (900 ± 10 °C) combustion of plants will lead to four characteristics: (1) the disappearance of odd-to-even predominance (OEP), (2) the forward shifts of main peak carbon, (3) the distribution of *n*-alkanes performing a similar trend as high maturity *n*-alkanes, and (4) appearance of the distribution of even-carbon dominant *n*-alkanes. Qiu et al. (2008) reported that the southern Junggar Basin had the low geothermal gradients and low maturity from the Lower Triassic to Middle Jurassic (Ro = 0.5–0.7% in most areas and <0.5% in some areas) as discussed in Section 5.1, thus the OEP characteristics cannot be attributed to geothermal effects. The values of OEP fluctuate below the Bed 43 and followed by a progressively decreasing trend, with average value of 2.33 (Fig. 3d). The values decrease to around 1 in the Bed 43 maintaining this level to the Bed 51 (i.e., around the DI zone). Sequence upwards, OEP values significantly increases above the Bed 51 up to average of 2.16 (Fig. 3d). In sum, the OEP parameters indicate a pre-existing thermal event at the stratigraphic interval of beds 43 to 51, before the depositional and burial. In addition, the fluctuating high abundance of coronene at the interval of beds 43 to 51 reflects the enhanced wildfires (Zhang et al., 2020) with peaks between the Bed 46 and Bed 49 (Fig. 2g). Thus, the DI zone is inferred to document the increased wildfire frequency.

The abundance *n*-alkanes series and conversion of *n*-alkanes peak patterns both can be witnessed to link with wildfires in the study section (Fig. 2 and Fig. 3). The two types of gas chromatography of samples show that the odd carbon predominance (mainly *n*C23 and *n*C25) disappears in the DI zone (Fig. 3). In these samples, *n*-alkanes distribution shows a modal distribution ranging from *n*C15 to *n*C33, with strong dominance of *n*C27 or *n*C29 for long-chain *n*-alkanes and *n*C16 or *n*C18 for short-chain *n*-alkanes, while short-chain *n*-alkanes presents an even-to-odd predominance (EOP) (Fig. 3). Bimodal *n*-alkanes could generally represent two main types of source input, i.e., both algae and terrestrial plants (Xu et al., 2015). The EOP of *n*-alkanes generally occurs due to: (1) the strongly reduced depositional environments, such as in deep marine sediments and salt rocks (Welte and Ebhardt, 1968; Wang et al., 2010a, 2010b), (2) specific bacteria and fungi input (Nguyen et al., 2000), and (3) thermal breakdown of long chain *n*-alkanes, commonly including intrusion baking, geothermal gradient and wildfires (Kuhn et al., 2009). However, there was no a strongly reduced depositional environment or exceptional occurrence of bacteria and fungi in the Haojiagou section (Fang et al., 2021). Moreover, the diagenetic geotherm stays almost same within 160-m-thick section, with neither magma intrusion baking beds and with the low maturity (Ro = 0.5–0.7% in most areas and <0.5% in some areas) in the southern Junggar Basin (Ding et al., 2003; Qiu et al., 2008). Thus, the potential impacts of reduced environments, bacteria and fungi input and geothermal degradation to abnormal EOP can be ruled out. A large amount of combustion products supplies primary inputs characterized in bimodal *n*-alkanes and front-peak carbon with EOP (Fig. 3).

5.3. Synchronous deforestation with global correlation of CAMP impacts

The CAMP volcanisms can be well correlated with the peaks of Hg/TOC (Ruhl et al., 2020; Lindström et al., 2021). Combined with the biostratigraphy and carbon isotope stratigraphy (see Fig. 4), the Hg/TOC peaks in the Haojiagou section constrains stratigraphic correlation against other classic ETE-TJB sections (Fig. 4) and links to the global influence of CAMP (Zhang et al., 2020; Ruhl et al., 2020). The peaks abundance of cadalene, retene, pimanthrene, furans and the abnormal interval of *n*-alkanes coincidently correspond to Hg/TOC peaks indicating the CAMP volcanisms labelled as V2 (Fig. 4) around the ETE-TJB interval. These characteristics in the Haojiagou section are well worldwide correlated to other sections. The records of coronene and furans in the Guangyuan and Hechuan sections of the Sichuan Basin (China) are well correlated with the Haojiagou section (Fig. 4). Moreover, coronene and retene can also be correlated in the Astartekloft, Greenland corresponding to Hg/TOC labelled as V2 (Fig. 4). The consistent global correlation suggests a synchronous response to the CAMP volcanisms in both terrestrial and marine ecosystems.

The ecosystem changes across the ETE-TJB interval are observed in key sections across the world, including terrestrial sections Guangyuan and Hechuan of the Sichuan Basin (southwest China) (Wang et al., 2010a, 2010b), Haojiagou, Junggar Basin (northwest China) (Lu and Deng, 2009; Sha et al., 2015) and Astartekloft (Greenland) (McElwain et al., 2009), and marine section Mariental (north Germany) (van de Schootbrugge et al., 2009). van de Schootbrugge et al. (2009) examined the stratigraphic micropalaeontology of the marine section at the Mariental, North Germany, and quantified floral changes. It is noted that the Triletes Beds show a dark spores zone which is consistent with the peak of coronene in the section, and is well correlated in other four terrestrial sections. The Hg/TOC content becomes particularly abundant (labelled as V2 in Fig. 4) and corresponds to the >4‰ negative carbon isotope excursion in the Astartekloft section, Greenland (McElwain et al., 2009). Anomaly high concentrations of retene (Fig. 4) related to gymnosperm resin derivatives suggest that the environmental stress factors lead to extinction of primary floras (Williford et al., 2014). The terrestrial sections at the Guangyuan and Hechuan, Sichuan Basin, southwest China also witness biomarkers coronene and furan (Fig. 4) for wildfires and environmental changes, outside CAMP region (Song et al., 2020). Of these sections, abundance of coronene suddenly increases in the ETE-TJB interval, and so as oxygenated PAHs with furan structure, which consistently demonstrate an increase of wildfire frequency and a floral destruction (Fig. 4).

With regard to wildfire activities, lava ignition of CAMP cannot directly affect Junggar Basin owing to >4000 km distance (Zhang et al., 2020; Song et al., 2020). However, the CAMP-derived 8000Gt (Gt = 10^9 t) of CO_2 (Beerling and Berner, 2002; McHone, 2003) injecting into the atmosphere can impact atmospheric cycles globally (Nomade et al., 2007; Whiteside et al., 2007; Schaller et al., 2011, 2012). Global warming at higher atmospheric CO_2 level may have increased by more than 4 °C (Landwehrs et al., 2020). According to modern atmospheric observation data, rising surface temperature will increase the moisture content of the troposphere and increase cloud (Reeve and Toumi, 1999). Every 1 °C increase in annual average temperature will increase the frequency of lightning by about 40% (Reeve and Toumi, 1999; Zhang et al., 2016), while lightning is one of the main causes of wildfires. On the other hand, volcanism is also known to be capable of releasing amounts of sulfur (Self et al., 2008; Jones et al., 2016) and the CAMP volcanisms released ~4600 Gt SO_2 (McHone, 2003).

Combined with the increase of PAHs content observed in terrestrial

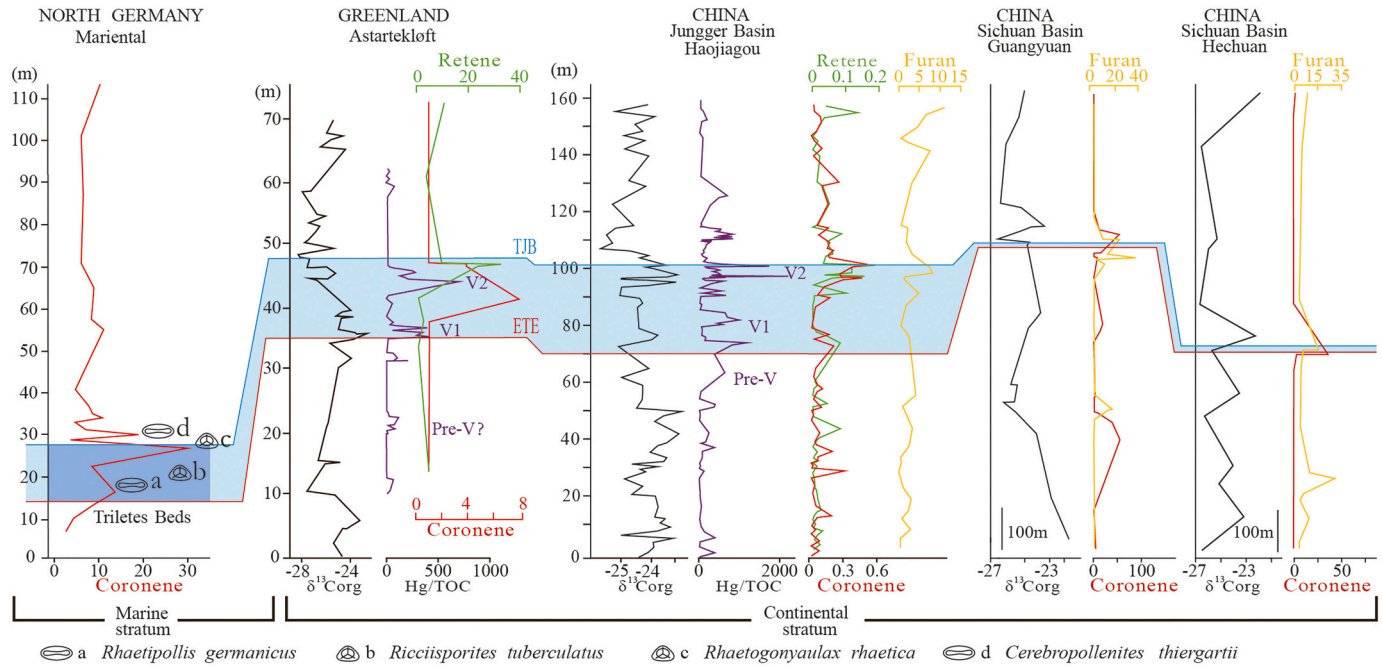

Fig. 4. Stratigraphic correlation of the Triassic-Jurassic transition in the Junggar Basin, northwest China is consistent with continental sections in the Astartekloft, Greenland (Williford et al., 2014), Guangyuan and Hechuan sections in the Sichuan Basin, China (Song et al., 2020) and shallow marine section in the Mariental, North Germany (van de Schootbrugge et al., 2009). The ETE boundary in the Mariental, North Germany was also defined by the characteristic late Triassic pollen (a) *Rhaetipollis germanicus*, where the first occurrence (FO) of pollen (d) *Cerebropollenites thiergartii* is located 3.2 m below the FO of the Triassic-Jurassic boundary marker ammonite *Psiloceras spelae* and 2.6 m above the ETE horizon in the Global Stratotype Sections and Point (GSSP) in Austria (Hillebrandt et al., 2013).

and marine sections across the world (van de Schootbrugge et al., 2009; Marynowski and Simoneit, 2009; Williford et al., 2014; Song et al., 2020; Zhang et al., 2020) (Fig. 4), the increased frequency of wildfires associated with deforestation across the ETE-TJB interval is likely to be on a global scale. However, mechanism of widespread deforestation with the synchronous wildfires widely taking place remains questionable. The enhanced wildfires owing to the global warming effects of CO_2 greenhouse (Reeve and Toumi, 1999; Beerling and Berner, 2002) could contribute to deforestation. Warmer temperatures can increase lightning frequency and directly ignite vegetation wildfires resulting into deforestation. On the contrary, the CAMP-derived sulfur injection would have a global impact because of its short residence years in the stratosphere (Robock, 2000) and transforming into acid rains to damage vegetations (Evans et al., 1977; Lal, 2016). If deforestation first took place due to the CAMP-derived global acid rains (McHone, 2003) and subsequent catastrophes of higher plants would rapidly oversupply moisture-free wood fuels with no time burial, which tends to cause enhanced wildfires. Moreover, the former mechanism is hard to explain why long-term strong greenhouse effects and more than 4 °C global warming due to high CO_2 contents stay until the Early Jurassic Hettangian (McElwain et al., 2009; Landwehrs et al., 2020) but just lead short-term wildfires (lasting ~270 kyr) across the ETE-TJB interval. In contrast, it would meet little difficulty for explaining the preceding floral death to cause the enhanced wildfires in short-time scale, according to the later mechanism. Concerning two alternative interpretations, we propose that the widespread deforestation initially occurred due to CAMP-derived acid rains and the large-scale demise of vegetation may have provided moisture-free fuels for wildfires, rather than intensive wildfires initially leading into the deforestation during the ETE-TJB period.

Notably, the abundant of retene and furans document a moderately increase of vegetation input in the zone RI in the Haojiagou section (Figs. 2 and 4), which suggest an ecosystem recovery with the aftermath of mass extinction. The retene at the Astartekloft, Greenland and furans at the Hechuan, China both show a slightly increasing tendency in the Early Jurassic (Fig. 4).

6. Conclusions

(1) Combined with the high-resolution biomarker datasets in this study and previous works at the Haojiagou section, the deforestation of higher plants took place in the Junggar Basin, northwest China recorded in the stratigraphic ETE-TJB interval. The deforestation was synchronous with the enhanced wildfires and also with the main stage of CAMP volcanisms in the Haojiagou section, Junggar Basin.

(2) The similar characteristics of deforestation indicated by biomarkers are witnessed in both other terrestrial and marine TJB sections across the world. Thus, the deforestation is inferred to be a global-scale event in the terrestrial ecosystems around the ETE-TJB period.

(3) The widespread deforestation in the ETE-TJB period could be triggered by the CAMP-derived acid rainfalls, and subsequently oversupplying dead plants were moisture-free to be ignited before buried. The deforestation is a main preceding reason rather than a consequence to enhance the wildfires in that period.

Declaration of Competing Interest

The authors declare that they have no known competing financial interests or personal relationships that could have appeared to influence the work reported in this paper.

Acknowledgements

We appreciate the two anonymous reviewers and Prof. Howard Falcon-Lang for their careful reading of our manuscript and for their constructive comments and suggestions. This project was supported by the National Natural Science Foundation of China (41502024, 42072148, 40372021, 41802118, 41730317), Exploration Fund of State Key Laboratory of Petroleum Resource and Prospecting, China University of Petroleum-Beijing (PRP/indep-4-1410) and Fund of Outstanding

Youth, China University of Petroleum-Beijing (2462014YJRC027). Linhao Fang and Guangli Wang would like to thank Lei Zhu, Jianfeng Zhang and Tiantian Li for their help with the experiments in China University of Petroleum-Beijing.

Appendix A. Supplementary data

Supplementary data to this article can be found online at https://doi.org/10.1016/j.palaeo.2022.111074.

References

van Aarssen, B.G.K., Cox, H.C., Hoogendoorn, P., de Leeuw, J.W., 1990. A cadinene biopolymer present in fossil and extant dammar resins as a source for cadinanes and bicadinanes in crude oils from South East Asia. Geochim. Cosmochim. Acta 54 (11), 3021–3031.

Bardhan, J.C., Sengupta, S.C., 1932. Resin acids. Part II. Synthesis of 1-methyl-7-iso-propylphenanthrene (retene). J. Chem. Soc. (Resumed) 2798–2800.

Beerling, D.J., Berner, R.A., 2002. Biogeochemical constraints on the Triassic-Jurassic boundary carbon cycle event. Glob. Biogeochem. Cy. 16 (3), 10-1–10-13.

Belcher, C.M., Mander, L., Rein, G., Jervis, F.X., Haworth, M., Hesselbo, S.P., Glasspool, I. J., McElwain, J.C., 2010. Increased fire activity at the Triassic/Jurassic boundary in Greenland due to climate-driven floral change. Nat. Geosci. 3 (6), 426–429.

Bonis, N.R., Kürschner, W.M., 2012. Vegetation history, diversity patterns, and climate change across the Triassic/Jurassic boundary. Paleobiology 38, 240–264.

Bordoloi, M., Shukla, V.S., Nath, S.C., Sharma, R.P., 1989. Naturally occurring cadinenes. Phytochemistry 28, 2007–2037.

Cai, Z.X., Chen, F.J., Jia, Z.Y., 2000. Types and tectonic evolution of Junger Basin. Earth Sci. Front. 7 (4), 431–440.

Deng, S.H., Lu, Y.Z., Fan, R., et al., 2010. The Jurassic System of Northern Xinjiang, China. University of Science and Technology of China Press, Hefei, 17–44, 187–192, 197–200.

Deng, S.H., Lu, Y.Z., Fan, R., Li, X., 2013. Terrestrial Triassic-Jurassic Boundary in China. J. Stratigr. 37 (4), 582–584.

Ding, A.N., Hui, R.Y., Zhang, Z.N., 2003. Hydrocarbon potential of Jurassic source rocks in the Junggar Basin, NW China. J. Pet. Geol. 26 (3), 307–324.

Dunhill, A.M., Foster, W.J., Sciberras, J., Twitchett, R.J., 2018. Impact of the late Triassic mass extinction on functional diversity and composition of marine ecosystems. Palaeontology 61, 133–148.

Eglinton, G., Murphy, M.T.J., 1969. Organic Geochemistry-Methods and Results. Springer Verlag, Berlin.

Eglinton, G., Scott, P.M., Besky, T., Burlingame, A.L., Calvin, M., 1964. Hydrocarbons of biological origin from a one-billion-old sediment. Science 145, 263–264.

Elias, V.O., de Barros, A.M.A., de Barros, A.B., Simoneit, B.R.T., Cardoso, J.N., 1997. Sesquiterpenoids in sediments of a hypersaline lagoon: A possible algal origin. Org. Geochem. 26 (11), 721–730.

Evans, L.S., Gmur, N.F., Costa, F.D., 1977. Leaf surface and histological perturbations of leaves of phaseolus vulgaris and helianthus annuus after exposure to simulated acid rain. Am. J. Bot. 64 (7), 903–913.

Fang, S.H., Guo, Z.J., Zhang, Z.C., Xu, H.M., Liu, L.J., 2004. Mesozoic tectonic evolution of Southern Junggar Basin, Northwestern China: constraints from stratigraphic and sedimentologic evidences. Geol. J. China Univ. 10 (4), 554–561.

Fang, L.H., Wang, G.L., Pieńkowski, G., Deng, S.H., Lu, Y.Z., Xu, W.M., Wu, H.C., Zheng, X.Y., Peng, B., Fang, Y.N., Lv, P.Z., Zhang, X.Y., 2022. The collapse of terrestrial ecosystems and abnormally high-temperature wildfires during end-Triassic mass extinction. Acta Sedimentol. Sin (under review).

Fang, Y.N., Wu, C.D., Wang, Y.Z., Jian, M.A., Zhou, T.Q., 2016. Lower to Middle Jurassic shallow-water delta types in the southern Junggar Basin and implications for the tectonic and climate (in Chinese with English abstract). Sci. Sin. Tech. 46, 737–756.

Fang, Y.N., Fang, L.H., Deng, S.H., Lu, Y.Z., Wang, B., Zhao, X.D., Wang, Y.Z., Zhang, H. C., Zhang, X.Z., Sha, J.G., 2021. Carbon isotope stratigraphy across the Triassic-Jurassic boundary in the high-latitude terrestrial Junggar Basin, NW China. Palaeogeogr. Palaeoclimatol. Palaeoecol. 577, 110559.

Fowell, S.J., Olsen, P.E., 1993. Time calibration of Triassic-Jurassic microfloral turnover, eastern North America. Tectonophysics 222, 361–369.

Greene, S.E., Martindale, R.C., Ritterbush, K.A., Bottjer, D.J., Corsetti, F.A., Berelson, W. M., 2012. Recognising Ocean acidification in deep time: an evaluation of the evidence for acidification across the Triassic-Jurassic boundary. Earth Sci. Rev. 113 (1–2), 72–93.

Grice, K., Backhouse, J., Alexander, R., Marshall, N., Logan, G.A., 2005. Correlating terrestrial signatures from biomarker distributions, δ13C, and palynology in fluvio-deltaic deposits from NW Australia (Triassic–Jurassic). Org. Geochem. 36 (10), 1347–1358.

Hautevelle, Y., Michels, R., Malartre, F., Trouiller, A., 2006. Vascular plant biomarkers as proxies for palaeoflora and palaeoclimatic changes at the Dogger/Malm transition of the Paris Basin (France). Org. Geochem. 37 (5), 610–625.

Hautmann, M., Benton, M.J., Tomašových, A., 2008. Catastrophic Ocean acidification at the Triassic-Jurassic boundary. N. Jb. Geol. Paläont. (Abh.) 249 (1), 119–127.

Hillebrandt, A.V., Krystyn, L., Kürschner, W.M., Bonis, N.R., Tomāsových, A., 2013. The Global Stratotype Sections and Point (GSSP) for the base of the Jurassic System at Kuhjoch (Karwendel Mountains, Northern Calcareous Alps, Tyrol, Austria). Episodes 36, 162–198.

Jaraula, C.M.B., Grice, K., Twitchett, R.J., Bottcher, M.E., Lemetayer, P., Dastidar, A.G., Opazo, L.F., 2013. Elevated pCO_2 leading to late Triassic extinction, persistent photic zone euxinia, and rising sea levels. Geology 41 (9), 955–958.

Jiang, N.H., Zhu, C.D., Gao, Y.J., 1994. Retene derived from non-high plants. Pet. Explor. Dev. 21 (5), 24–28.

Jiang, C.Q., Alexander, R., Kagi, R.I., Murray, A.P., 1998. Polycyclic aromatic hydrocarbons in ancient sediments and their relationships to palaeoclimate. Org. Geochem. 29 (5), 1721–1735.

Jones, M.T., Jerram, D.A., Svensen, H.H., Grove, C., 2016. The effects of large igneous provinces on the global carbon and sulphur cycles. Palaeogeogr. Palaeoclimatol. Palaeoecol. 441, 4–21.

Kaiho, K., Oshima, N., Adachi, K., Adachi, Y., Mizukami, T., Fujibayashi, M., Saito, R., 2016. Global climate change driven by soot at the K-Pg boundary as the cause of the mass extinction. Sci. Rep. 6 (1), 1095–1108.

Kuhn, T.K., Krull, E.S., Bowater, A., Grice, K., Gleixner, G., 2009. The occurrence of short chain n-alkanes with an even over odd predominance in higher plants and soils. Org. Geochem. 41 (2), 88–95.

Lal, N., 2016. Effects of acid rain on plant growth and development. E J. Surf. Sci. Nanotechnol. 11 (5), 85–108.

de Lamotte, D.F., Fourdan, B., Leleu, S., Leparmentier, F., Clarens, P., 2015. Style of rifting and the stages of Pangea breakup. Tectonics 34 (5), 1009–1029.

Landwehrs, J.P., Feulner, G., Hofmann, M., Petri, S., 2020. Climatic fluctuations modeled for carbon and sulfur emissions from end-Triassic volcanism. Earth Planet. Sci. Lett. 537, 116174.

Li, M.R., Zhou, H.R., Wang, X.L., Liu, Z.R., 2007. Braided-river delta deposition of the Badaowan Formation of lower Jurassic in Haojiagou section, southern Junggar Basin. Petrol. Geol. Recov. Eff. 14 (3), 41–45.

Lindström, S., Erlström, M., 2006. The late Rhaetian transgression in southern Sweden: Regional (and global) recognition and relation to the Triassic-Jurassic boundary. Palaeogeogr. Palaeoclimatol. Palaeoecol. 241 (3), 339–372.

Lindström, Sofie, Callegaro, Sara, Davies, Joshua, Tegner, Christian, van de Schootbrugge, Bas, Pedersen, Gunver K., Youbi, Nasrrddine, Sanei, Hamed, Marzoli, Andrea, 2021. Tracing volcanic emissions from the Central Atlantic Magmatic Province in the sedimentary record. Earth Sci. Rev. 212, 103444.

Lu, Y.Z., Deng, S.H., 2009. Palaeoclimate around the Triassic-Jurassic Boundary in southern margin of Junggar Basin. J. Palaeogeogr. 11 (6), 652–660.

Lucas, S.G., Tanner, L.H., 2007. The nonmarine Triassic-Jurassic boundary in the Newark Supergroup of eastern North America. Earth Sci. Rev. 84, 1–20.

Marynowski, L., Simoneit, B.R.T., 2009. Widespread upper Triassic to lower Jurassic wildfire records from Poland: evidence from charcoal and pyrolytic polycyclic aromatic hydrocarbons. Palaios 24 (12), 785–798.

McElwain, J.C., Beerling, D.J., Woodward, F.I., 1999. Fossil Plants and Global Warming at the Triassic-Jurassic Boundary. Science 285 (5432), 1386–1390.

McElwain, J.C., Popa, M.E., Hesselbo, S.P., Haworth, M., Surlyk, F., 2007. Macroecological responses of terrestrial vegetation climatic and atmospheric change across the Triassic/Jurassic boundary in East Greenland. Paleobiology 33, 547–573.

McElwain, J.C., Wagner, P.J., Hesselbo, S.P., 2009. Fossil plant relative abundances indicate sudden loss of late Triassic biodiversity in East Greenland. Science 324 (5934), 1554–1556.

Mcghee, G.R., Clapham, M.E., Sheehan, P.M., Bottjer, D.J., Droser, M.L., 2013. A new ecological-severity ranking of major Phanerozoic biodiversity crises. Palaeogeogr. Palaeoclimatol. Palaeoecol. 370, 260–270.

McHone, J.G., 2003. Volatile emissions of Central Atlantic Magmatic Province basalts: Mass assumptions and environmental consequences. In: Hames, W.E., et al. (Eds.), The Central Atlantic Magmatic Province: American Geophysical Union Monograph, vol. 136, pp. 241–254.

Mizukami, T., Kaiho, K., Oba, M., 2013. Significant changes in land vegetation and oceanic redox across the cretaceous/Paleogene boundary. Palaeogeogr. Palaeoclimatol. Palaeoecol. 369, 41–47.

Nakamura, H., Sawada, K., Takahashi, M., 2010. Aliphatic and aromatic terpenoid biomarkers in cretaceous and Paleogene angiosperm fossils from Japan. Org. Geochem. 41 (9), 975–980.

Nguyen, Tu, Derenne, S., Largeau, C., Mariotti, A., Bocherens, H., Pons, D., 2000. Effects of fungal infection on lipid extract composition of higher plant remains: comparison of shoots of a Cenomanian conifer, uninfected and infected by extinct fungi. Org. Geochem. 31 (12), 1743–1754.

Nguyen, Tu, Derenne, S., Largeau, C., Mariotti, A., Bocherens, H., 2003. Comparison of leaf lipids from a fossil ginkgoalean plant and its extant counterpart at two degradation stages: diagenetic and chemotaxonomic implications. Rev. Palaeobot. Palynol. 124 (1), 63–78.

Nomade, S., Knight, K., Beutel, E., Renne, P., Verati, C., Feraud, G., Marzoli, A., Youbi, N., Bertrand, H., 2007. Chronology of the Central Atlantic Magmatic Province: implications for the Central Atlantic rifting processes and the Triassic-Jurassic biotic crisis. Palaeogeogr. Palaeoclimatol. Palaeoecol. 244 (1–4), 326–344.

O'Malley, V.P., Burke, R.A., Schlotzhauer, W.S., 1997. Using GC-MS/Combustion/IRMS to determine the 13C/12C ratios of individual hydrocarbons produced from the combustion of biomass materials-application to biomass burning. Org. Geochem. 27 (7), 567–581.

Peace, A., Phethean, J., Franke, D., Foulger, G., Dore, A., 2019. A review of Pangaea dispersal and large igneous provinces – in search of a causative mechanism. Earth Sci. Rev. 102902.

Peters, K.E., Walters, C.C., Moldowan, J.M., 2005. The Biomarker Guide, vol. 2. Cambridge University Press.

Petersen, H.I., Lindström, S., 2012. Synchronous Wildfire Activity Rise and Mire Deforestation at the Triassic–Jurassic Boundary. PLoS One 7 (10), e47236.

Pieńkowski, G., Niedźwiedzki, G., Waksmundzka, M., 2012. Sedimentological, palynological and geochemical studies of the terrestrial Triassic-Jurassic boundary in northwestern Poland. Geol. Mag. 149 (2), 308–332.
Qiu, N.S., Zhang, Z.H., Xu, E.S., 2008. Geothermal regime and Jurassic source rock maturity of the Junggar Basin, northwest China. J. Asian Earth Sci. 31 (4–6), 464–478.
Radke, M., Vriend, S.P., Ramanampisoa, L.R., 2000. Alkyldibenzofurans in terrestrial rocks: influence of organic facies and maturation. Geochim. Cosmochim. Acta 64 (2), 275–286.
Raup, D.M., Sepkoski, J.J., 1982. Mass extinctions in the marine fossil record. Science 215 (4539), 1501–1503.
Reeve, N., Toumi, R., 1999. Lightning activity as an indicator of climate change. Q. J. R. Meteorol. Soc. 125 (555), 893–903.
Robock, A., 2000. Volcanic eruptions and climate. Rev. Geophys. 38, 191–219.
Ruhl, M., Hesselbo, S.P., Al-Suwaidi, A., Jenkyns, H.C., Damborenea, S.E., Manceñido, M.O., Storm, M., Mather, T.A., Riccardi, A.C., 2020. On the onset of Central Atlantic Magmatic Province (CAMP) volcanism and environmental and carbon-cycle change at the Triassic–Jurassic transition (Neuquén Basin, Argentina). Earth Sci. Rev. 208, 103229.
Schaller, M.F., Wright, J.D., Kent, D.V., 2011. Atmospheric pCO_2 perturbations associated with the Central Atlantic Magmatic Province. Science 331, 1404–1409.
Schaller, M.F., Wright, J.D., Kent, D.V., Olsen, P.E., 2012. Rapid emplacement of the Central Atlantic Magmatic Province as a net sink for CO_2. Earth Planet. Sci. Lett. 323-324, 27–39.
van de Schootbrugge, B., Quan, T.M., Lindström, S., Püttmann, W., Heunisch, C., Pross, J., Fiebig, J., Petschick, R., Röhling, H.-G., Richoz, S., Rosenthal, Y., Falkowski, P.G., 2009. Floral changes across the Triassic/Jurassic boundary linked to flood basalt volcanism. Nat. Geosci. 2 (8), 589–594.
Self, S., Blake, S., Sharma, K., Widdowson, M., Sephton, S., 2008. Sulfur and chlorine in late cretaceous Deccan magmas and eruptive gas release. Science 319, 1654–1657.
Sephton, M.A., Looy, C.V., Veefkind, R.J., Visscher, H., Brinkhuis, H., de Leeuw, J.W., 1999. Cyclic diaryl ethers in a late Permian sediment. Org. Geochem. 30 (4), 267–273.
Sha, J.G., Olsen, P.E., Pan, Y.H., Xu, D.Y., Wang, Y.Q., Zhang, X.L., Yao, X.G., Vajda, V., 2015. Triassic-Jurassic climate in continental high-latitude Asia was dominated by obliquity-paced variations (Junggar Basin, Ürümqi, China). Proc. Natl. Acad. Sci. U. S. A. 112 (12), 3624–3629.
Simoneit, B.R.T., 1977. Diterpenoid compounds and other lipids in deep-sea sediments and their geochemical significance. Geochim. Cosmochim. Acta 41 (4), 463–476.
Simoneit, B.R.T., Grimalt, J.O., Wang, T.G., Cox, R.E., Hatcher, P.G., Nissenbaum, A., 1986. Cyclic terpenoids of contemporary resinous plant detritus and of fossil woods, ambers and coals. Org. Geochem. 10 (4–6), 877–889.
Simoneit, B.R.T., Rogge, W.F., Lang, Q., Jaffé, R., 2000. Molecular characterization of smoke from campfire burning of pine wood (Pinus elliottii). Chemosp. Glob. Change Sci. 2 (1), 107–122.
Song, Y., Algeo, T.J., Wu, W.J., Luo, G.M., Li, L.Q., Wang, Y.D., Xie, S.C., 2020. Distribution of pyrolytic PAHs across the Triassic-Jurassic boundary in the Sichuan Basin, southwestern China: evidence of wildfire outside the Central Atlantic Magmatic Province. Earth Sci. Rev. 201 (C), 102970.
Stefanova, M., Oros, D.R., Otto, A., Simoneit, B.R.T., 2002. Polar aromatic biomarkers in the Miocene Maritza-East lignite, Bulgaria. Org. Geochem. 33 (9), 1079–1091.
Steinthorsdottir, M., Jeram, A.J., Mcelwain, J.C., 2011. Extremely elevated CO_2 concentrations at the Triassic/Jurassic boundary. Palaeogeogr. Palaeoclimatol. Palaeoecol. 308 (3), 418–432.
Wakeham, S.G., Schaffner, C., Giger, W., 1980. Poly cyclic aromatic hydrocarbons in recent lake sediments-II. Compounds derived from biogenic precursors during early diagenesis. Geochim. Cosmochim. Acta 44 (3), 415–429.
Wang, Y.L., Fang, X.M., Zhang, T.W., Li, Y.M., Wu, Y.Q., He, D.X., Wang, Y.X., 2010a. Predominance of even carbon-numbered n-alkanes from lacustrine sediments in Linxia Basin, NE Tibetan Plateau: Implications for climate change. Appl. Geochem. 25 (10), 1478–1486.
Wang, Y.D., Fu, B.H., Xie, X.P., Huang, Q.S., Li, K., Li, G., Liu, Z.S., Yu, J.X., Pan, Y.H., Tian, N., Jiang, Z.K., 2010b. The Terrestrial Triassic and Jurassic Systems in the Sichuan Basin, China. University of Science and Technology of China Press, Hefei, China, 216 pp. (in Chinese and English).
Welte, D.H., Ebhardt, G., 1968. Distribution of long chain n-paraffIns and n-fatty acids in sediments from the Persian Gulf. Geochim. Cosmochim. Acta 32 (4), 465–466.
Whiteside, J.H., Olsen, P.E., Kent, D.V., Fowell, S.J., Et-Touhami, M., 2007. Synchrony between the Central Atlantic magmatic province and the Triassic-Jurassic mass-extinction event? Palaeogeogr. Palaeoclimatol. Palaeoecol. 244 (1), 345–367.
Wignall, P.B., Atkinson, J.W., 2020. A two-phase end-Triassic mass extinction. Earth Sci. Rev. 208, 103282.
Williford, K.H., Grice, K., Holman, A., McElwain, J.C., 2014. An organic record of terrestrial ecosystem collapse and recovery at the Triassic–Jurassic boundary in East Greenland. Geochim. Cosmochim. Acta 127, 251–263.
Xu, M.N., Wang, Y.H., Yang, H., Xie, B., Niu, X.Y., 2015. Modern climate and vegetation variability recorded in organic compounds and carbon isotopic compositions in the Dianchi Watershed. Environ. Sci. Pollut. Res. Int. 22 (18), 14314–14324.
Zhang, X.Q., Zhang, G.Q., Xi, S.N., Li, L.Q., Deng, C.T., Wang, Y., Zhou, N., Wang, Y.D., Song, Y., 2016. Wildfire event at the Triassic/Jurassic boundary: Approaches, progress, and perspective. Acta Palaeontol. Sin. 55 (3), 331–345.
Zhang, X.Z., Fang, L.H., Wu, T., Miao, Y.F., Zhang, M.Z., Wang, X.L., Lv, P.Z., He, X.J., Qiu, R.Y., Yang, H., Ren, J.H., 2022. Palynological assemblages and palaeoclimate across the Triassic-Jurassic boundary in the Haojiagou section, southern Junggar Basin. Chin. J. Geol. (Chinese with English abstract) Accepted.
Zhang, X.Z., Lv, P.Z., Fang, L.H., Yang, H., Deng, S.H., Lu, Y.Z., Fang, Y.N., Zhang, X.Y., Huang, R.T., Liang, J.B., Shi, S.B., 2020. Wildfire records across the Triassic-Jurassic boundary in the southern margin of the Junggar Basin and global correlations. Acta Sedimentol. Sin. https://doi.org/10.14027/j.issn.1000-0550.2020.103.
Zhou, W., Wang, R.Y., Radke, M., Wu, Q.Y., Sheng, G.Y., Liu, Z.L., 2000. Retene in pyrolysates of algal and bacterial organic matter. Org. Geochem. 31 (7), 757–762.